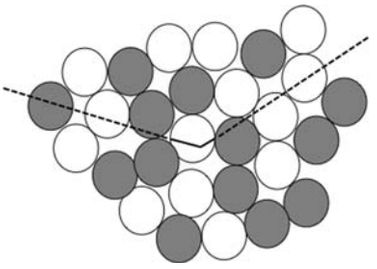

Figure 3.2.3
Sketch illustrating an X-ray propagating through a mixture of two kinds of particles.

This leads to a weaker observed reflection from a phase a with larger absorption constant μ_a if the particle size is an appreciable fraction of $1/(\mu_a - \bar{\mu})$.

Averaging over the particle volume, we see that the observed intensity of phase a will be lowered from its value in a fine powder by a factor

$$\tau = V_a^{-1} \int \exp[-(\mu_a - \overline{\mu})x]\, \mathrm{d}V_a,$$

where the integral is taken over one representative grain of phase a. This is exactly the integral of equation (3.2.15), and if one assumes monodisperse spherical particles, it is tabulated in *International Tables for Crystallography*, Volume C, Section 6.3.3.2 and elsewhere, with $\mu_a - \bar{\mu}$ replacing μ. One hitch is that the tabulations are for $\mu > 0$, whereas $\mu_a - \bar{\mu} < 0$ for the less absorbing phases in a mixture. Brindley handles this with a series expansion and provides a table of τ *versus* $(\mu_a - \bar{\mu})R$.

By way of illustration, consider a mixture of equal weight fractions of corundum, magnetite and zircon powders, analysed with Cu $K\alpha$ radiation. Fig. 3.2.4 shows the weight fractions that would be measured from such a sample as a function of particle radius (assumed equal for all three phases). In this case, microabsorption biases the result by about 10% for particles of 10 μm diameter, and misses by a factor of two if the diameter is 70 μm.

In considering microabsorption, there are several important points to note. This entire analysis is only valid for $\mu R \ll 1$, since otherwise the concept of an average absorption length becomes ill defined. That means that the Brindley analysis breaks down precisely when it becomes significant. Of course, the Brindley assumption of monodisperse spherical particles is unrealistic for most real samples. Both the surface roughness and Brindley corrections depend on diffraction angle as well as μR, but, as noted above, for moderate absorption, the angle dependence appears as an effective Debye–Waller factor. The parameter R is the radius of the grain of material, which is commonly very much larger than the size of a coherently diffracting region; a Scherrer analysis of particle size through line broadening does not provide a useful estimate of R. Most importantly, unless one has an accurate independent measurement of the size and shape of the grains, microabsorption corrections should be taken as a sign of impending trouble, not a quantitative correction.

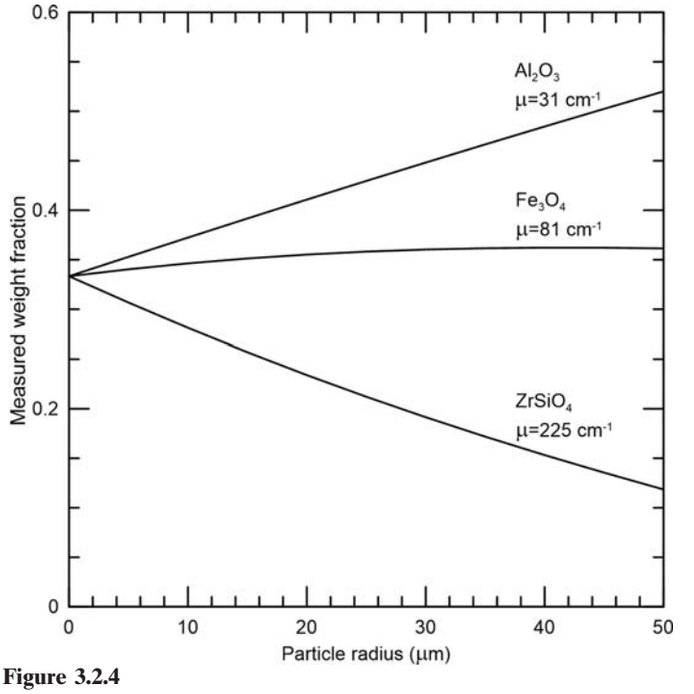

Figure 3.2.4
Weight fractions that would be measured from a mixture of equal parts of three phases with Cu $K\alpha$ radiation.

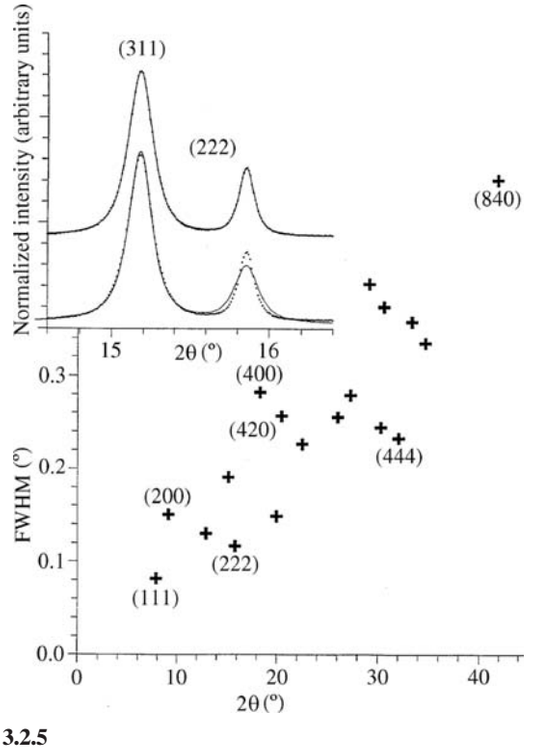

Figure 3.2.5
Diffraction peak width *versus* diffraction angle from a powder pattern of face-centred cubic Rb_3C_{60} (Stephens, 1999). The inset at the top shows a limited range of the data, fitted by a model with two different peak widths (upper trace) and with the widths constrained to be equal (lower trace).

3.2.3.4. *Anisotropic strain broadening*

Strain broadening is often observed not to be monotonically dependent on the magnitude of the d-spacing, but to have a more complicated dependence on the direction of the diffraction vector **G**. An illustration of the effect in cubic Rb_3C_{60} is shown in Fig. 3.2.5 (Stephens, 1999). The lower part of the figure shows an apparently irregular trend of diffraction peak widths on diffraction angle 2θ.

Whatever the nature of random internal stresses and strains, it can be argued on general grounds that strain broadening depends on a combination of fourth-rank tensors. On the assumption that the distribution of random strains is Gaussian, each diffraction peak has Gaussian shape, and the variance of the inverse d-spacing squared is a quartic form in the reflection indices (hkl). This can be expressed as

$$\sigma^2 = \langle d_{hkl}^{-4}\rangle - \langle d_{hkl}^{-2}\rangle^{-2} = \sum_{HKL} S_{HKL} h^H k^K l^L, \qquad (3.2.17)$$

where the sum is over terms with $H + K + L = 4$. This leads to a contribution to the width of a diffraction peak proportional to $\Gamma_{2\theta} = d^2\sqrt{\sigma^2}\tan\theta$ for angle-dispersive measurements, and $\Gamma_t = td^2\sqrt{\sigma^2}$ for time-of-flight neutron measurements. Strain broadening in real samples frequently leads to peak shapes that are closer to Lorentzian than Gaussian, and the justification of this expression breaks down because the second moment of the distribution of d^{-2} is then not defined. Nevertheless, this method is often successful at modelling the phenomenology of anisotropic peak broadening.

The parameters S_{HKL} arise from the nature of the strain and the values of elastic constants for any particular sample. Typically, they must therefore be regarded as phenomenological, and can be adjusted in fitting a model to observed data. They are constrained by the symmetry of the Laue group of the sample, which leads to restrictions on the S_{HKL} terms for the various Laue classes, listed in Table 3.2.1 (Popa, 1998).

Table 3.2.1
Restrictions and reflections of anisotropic strain parameters for the various Laue classes

$\bar{3}, \bar{3}m1, \bar{3}1m$: hexagonal indices.

Class	$\langle 1/d^2\rangle^2$
$\bar{1}$	$S_{400}h^4 + S_{040}k^4 + S_{004}l^4 + S_{220}h^2k^2 + S_{202}h^2l^2 + S_{022}k^2l^2 + S_{310}h^3k + S_{130}hl^3 + S_{301}h^3l + S_{103}hl^3 + S_{031}k^3l + S_{013}kl^3 + S_{211}h^2kl + S_{121}hk^2l + S_{112}hkl^2$
$2/m$ (b-axis unique)	$S_{400}h^4 + S_{040}k^4 + S_{004}l^4 + S_{220}h^2k^2 + S_{202}h^2l^2 + S_{022}k^2l^2 + S_{301}h^3l + S_{103}hl^3 + S_{121}hk^2l$
$2/mmm$	$S_{400}h^4 + S_{040}k^4 + S_{004}l^4 + S_{220}h^2k^2 + S_{202}h^2l^2 + S_{022}k^2l^2$
$4/m$	$S_{400}(h^4 + k^4) + S_{004}l^4 + S_{220}h^2k^2 + S_{202}(h^2 + k^2)l^2 + S_{310}(h^3k - hk^3)$
$4/mmm$	$S_{400}(h^4 + k^4) + S_{004}l^4 + S_{220}h^2k^2 + S_{202}(h^2 + k^2)l^2$
$\bar{3}$	$S_{400}(h^2 + k^2 + hk)^2 + S_{202}(h^2 + k^2 + hk)l^2 + S_{004}l^4 + S_{211}(h^3 - k^3 + 3h^2k)l + S_{121}(-h^3 + k^3 + 3hk^2)l$
$\bar{3}m1$	$S_{400}(h^2 + k^2 + hk)^2 + S_{202}(h^2 + k^2 + hk)l^2 + S_{004}l^4 + S_{301}(2h^3 + 3h^2k - 3hk^2 - 2k^3)l$
$\bar{3}1m$	$S_{400}(h^2 + k^2 + hk)^2 + S_{202}(h^2 + k^2 + hk)l^2 + S_{004}l^4 + S_{211}(h^2k + hk^2)l$
Hexagonal	$S_{400}(h^2 + k^2 + hk)^2 + S_{202}(h^2 + k^2 + hk)l^2 + S_{004}l^4$
Cubic	$S_{400}(h^4 + k^4 + l^4) + S_{220}(h^2k^2 + h^2l^2 + k^2l^2)$

3.2.3.5. *Preferred orientation (texture)*

The discussion of diffraction-peak intensities in Section 3.2.2.2 above presumes that the sample is a random powder, with every orientation equally probable. Real samples frequently exhibit some deviation from that ideal case, perhaps because of the way that grains of platy or acicular (needle-like) habit settle into a sample holder, or because a solid polycrystalline sample crystallized or grew anisotropically, or was formed or worked as a solid. The latter case is generally called texture, and can provide a fruitful basis for understanding the history or mechanical properties of a sample. The topic is further discussed in Chapter 5.3 of this volume. For the present purposes, deviation from a collection of randomly oriented grains will be regarded as an artifact to be minimized and/or modelled.

The distribution of orientations of crystallites in a sample can be studied using pole figures. For a given reflection **G**, the pole figure is defined as the probability density over a spherical surface that **G** falls in a particular direction relative to the sample. For a random powder, all pole figures would be uniform; for a single crystal, each pole figure would be a set of delta functions. Modelling of preferred orientation in the sample is accomplished by multiplying the theoretical intensity by the pole-figure density in the direction of the diffraction vector. Here we discuss two different treatments of preferred orientation.

The symmetrized spherical-harmonic approach follows Järvinen (1993), considering samples that are axially symmetric about some axis **P**. Experimentally, this can be ensured by rotating the sample about **P** during data collection. Take α to be the angle between **P** and the diffraction vector: α is zero for a conventional symmetrical flat plate and 90° for Debye–Scherrer geometry.

For a given reflection hkl, the polar-axis density in the diffraction direction may be expanded in spherical harmonics as

$$A(hkl, \alpha) = \sum_{ij} C_{ij} Y_{ij}(\theta_{hkl}, \varphi_{hkl}) P_i(\cos\alpha),$$

where Y_{ij} and P_i are the usual spherical harmonics and Legendre polynomials, and θ_{hkl} and φ_{hkl} are the spherical coordinates of the hkl reflection relative to some chosen axis of the crystal.

In general, there will be several reflections equivalent to hkl by the Laue symmetry of the crystalline phase, and so symmetry-adapted functions should replace the spherical harmonics in the above equation. Only even orders i are considered, because of the inversion symmetry of diffraction (neglecting imaginary atomic scattering amplitudes). The Laue symmetry of the crystalline phase implies that certain of the harmonics are zero; see the original article by Järvinen (1993) for explicit functional forms of the harmonics and a tabulation of which are allowed for each Laue group.

The second approach considered here is the widely used March (1932)–Dollase (1986) model, which is applicable to the most common powder-diffraction sample geometries of axial symmetry either along the diffraction vector or perpendicular to the diffraction plane, for samples whose preferred orientation arises from the settling of either disc- or rod-shaped crystallites in the sample holder. The cylinder axis **H** governs the preferred orientation. For any Bragg reflection **G**, the pole density in the diffraction direction is hypothesized to be a particular function of the angle α between **H** and **G**, *viz.*

$$A(G) = (R^2\cos^2\alpha + \sin^2\alpha/R)^{-3/2}.$$

Here R is a parameter describing the degree of preferred orientation; it is less than unity for maximum pole density at α = 0, *i.e.*, **H** ∥ **G**, as would be found for disc-like samples preferentially lying in the reflection plane. $R > 1$ corresponds to maximum pole density at $\alpha = 90°$, as might be found for acicular crystallites in either a flat-plate or Debye–Scherrer geometry. The particular functional form has some theoretical justification as a model for grain rotation in settling of a granular sample, as well as being properly normalized, suitable for oblate or prolate grains with a single parameter, and in agreement with pole distributions observed in many samples. To apply this model to powder-diffraction data, one must find the appropriate axis **H**, either through prior knowledge of growth habit or by trial and error.

3.2.3.6. *Extinction*

The analysis of diffracted intensities in this chapter has been premised on the assumption that the diffracted beam produced by each crystallite is much weaker than the incident beam, known